Chemical Science

ROYAL SOCIETY OF CHEMISTRY

EDGE ARTICLE

View Article Online
View Journal | View Issue

Cite this: *Chem. Sci.*, 2023, **14**, 8305

All publication charges for this article have been paid for by the Royal Society of Chemistry

Received 19th April 2023
Accepted 28th June 2023

DOI: 10.1039/d3sc02025h

rsc.li/chemical-science

Chemical sensors for imaging total cellular aliphatic aldehydes in live cells†

Rachel Wills, ‡[a] Jonathan Farhi, ‡[b] Patrick Czabala,[a] Sophia Shahin,[a] Jennifer M. Spangle[b] and Monika Raj *[a]

Aliphatic aldehydes are reactive electrophilic carbonyls that cross-link with DNA and proteins leading to cellular toxicity and disease pathogenesis. This toxicity is due to the cooperative effect of multiple aldehydes *via* a common mechanism. Therefore, live-cell imaging of total aliphatic aldehydes, small-to-long chain (C_1–C_{10}), is highly desired to decipher their physiological and pathological functions. However, sensors for imaging total cellular aliphatic aldehydes are currently lacking despite their high concentrations (~80 to >500 μM) inside cells. Herein, we report chemical sensors that generate a benzimidazole moiety upon reaction with aliphatic aldehydes of different chain lengths (C_1–C_{10}), resulting in turn-on fluorescence. These sensors exhibit high quantum yields, high dynamic range, and enable the quantification of changes in both the exogenous administration of aldehydes and endogenous real-time formation of aliphatic aldehydes in live mammalian cells. This tool has great potential to transform aldehyde research by illuminating cellular metabolites that have remained elusive in living systems.

Introduction

There is a broad presence of aliphatic aldehydes in the environment that humans are exposed to on daily basis.[1] Additionally, cellular processes including the metabolism of amino acids, carbohydrates, lipids, steroids, and vitamins, and oxidative stress generate a variety of small-to-long (C_1–C_{10}) chain aliphatic aldehydes.[2] The half-lives of these aldehydes range from minutes to hours and their free diffusion in cells contributes to cytotoxicity. This is due to their rapid reactivity with various biological nucleophiles including lipids, proteins, enzymes, and DNA.[3] The physiological abundance of aliphatic aldehydes varies from ~80 to >500 μM and can lead to effects on metabolic and cellular processes.[4] Pathological levels of these aldehydes vary from low to high millimolar (~100 mM) and have been increasingly appreciated in various diseases.[4] For example, aldehydes can directly crosslink with DNA, causing DNA damage in the form of mutations (*e.g.*, G-to-T transversion), reduction of DNA repair capacity, and chromosomal aberrations. The damage to DNA by aldehydes is cytotoxic and carcinogenic and is known to contribute to cardiovascular and neurological disorders such as Alzheimer's disease (AD).[5] As a result of their cytotoxicity, the abundance of many aldehydes is tightly regulated by enzymes in the aldehyde dehydrogenase (ALDH) superfamily, which convert them into nontoxic acids.[6] However, disease states or mutations in ALDH enzymes can lead to the accumulation of toxic aldehydes. For example, a missense mutation (E487K) in ALDH2, designated as the ALDH2*2 allele, leads to a significant decrease in the enzymatic ability to convert aldehydes into nontoxic acids and affects approximately >600 million people worldwide. The mutation that causes the defective ALDH2*2 enzyme is more common than other highly studied genetic missense mutations, including those that cause sickle cell anemia, cystic fibrosis, and glucose-6-phosphate dehydrogenase (G6PD) deficiency.[7] For this reason, it is imperative to develop tools to accurately monitor aldehydes in a biological environment. However, a major challenge in deciphering the biological and pathological roles of aliphatic aldehydes is the real-time measurement of their concentrations, longevity, and subcellular localization in living cells.

Cellular aldehydes are traditionally quantified using cell lysate by mass-coupled gas or liquid chromatography[8] and colorimetric/fluorometric kits.[9] These methods require the lysis of cellular membranes to release the aldehydes. Destruction of the membrane creates three issues: first, it decreases the aldehyde levels due to the volatile nature of short chain aliphatic aldehydes.[10] Second, it increases the production of aldehydes due to the oxidative stress that occurs during cell death.[2] Lastly, it results in the loss of spatio-temporal information. These limitations lead to the inaccurate analysis of cellular aldehyde

[a]*Department of Chemistry, Emory University, Atlanta, GA, USA. E-mail: monika.raj@emory.edu*

[b]*Department of Radiation Oncology, Winship Cancer Institute of Emory University School of Medicine, Atlanta, GA, USA*

† Electronic supplementary information (ESI) available. See DOI: https://doi.org/10.1039/d3sc02025h

‡ R. W. and J. F. contributed equally to this project.

levels, precluding the detection of cell-to-cell variability in aldehyde concentrations and the real time monitoring of aldehyde levels in live cells.

In contrast, fluorescent sensors using aza-cope rearrangement and Schiff base condensation of aldehydes with amines, hydrazines, or hydrazides represent a powerful, non-invasive tool for the real-time monitoring of endogenous aldehydes in live cells. However, these methods are limited to detecting only small-chain aliphatic aldehydes like formaldehyde (C1) and acetaldehyde (C2), or present inaccurate quantification based on their reversible nature (Fig. 1a).[11] Humans are consistently exposed to a complex mixture of aldehydes from both exogenous sources and endogenous metabolic pathways. These different aldehydes interact additively by a common mechanism thus contributing to cellular toxicity in a synergistic manner.[12] Therefore, imaging and determining total aliphatic aldehyde concentrations in cells would provide accurate monitoring of cellular toxicity. Currently, no irreversible fluorescent sensors are available for the real-time imaging, detection, and quantification of total aliphatic aldehydes, including medium-to-long-chain aliphatic aldehydes (C3–C10) in live cells.[11] Previously, 3,4-phenyldiamine-BODIPY sensors have been reported to detect the concentrations of nitric oxide (NO) and methyl glyoxal (MGO) in live cells by the formation of benzotriazole and quinoxaline products, respectively.[13,14] The detection of aliphatic aldehydes by these sensors was not determined at that time. We herein report that 3,4-phenyldiamine-BODIPY sensors react rapidly with aliphatic aldehydes (C_1–C_{10}), irrespective of their chain length, to form an irreversible benzimidazole moiety that results in turn-on fluorescence. We repurposed the membrane-permeable and photostable 3,4-phenyldiamine-BODIPY sensors to detect and monitor changes in small-to-long chain aliphatic aldehyde levels in live cells, without interference from other biological metabolites.

These 3,4-phenyldiamine-BODIPY sensors do not require catalysts and are non-cytotoxic, which is in contrast to the known hydrazine-based DarkZone[11f] and naphthalimide sensors.[11e] Our sensors display high sensitivity (26-fold increase in fluorescence), fast reaction kinetics ($k = 0.0103\ s^{-1}$), and a high dynamic range (2 μM to 100 mM) allowing for the quantification and real-time monitoring of changes in the endogenous

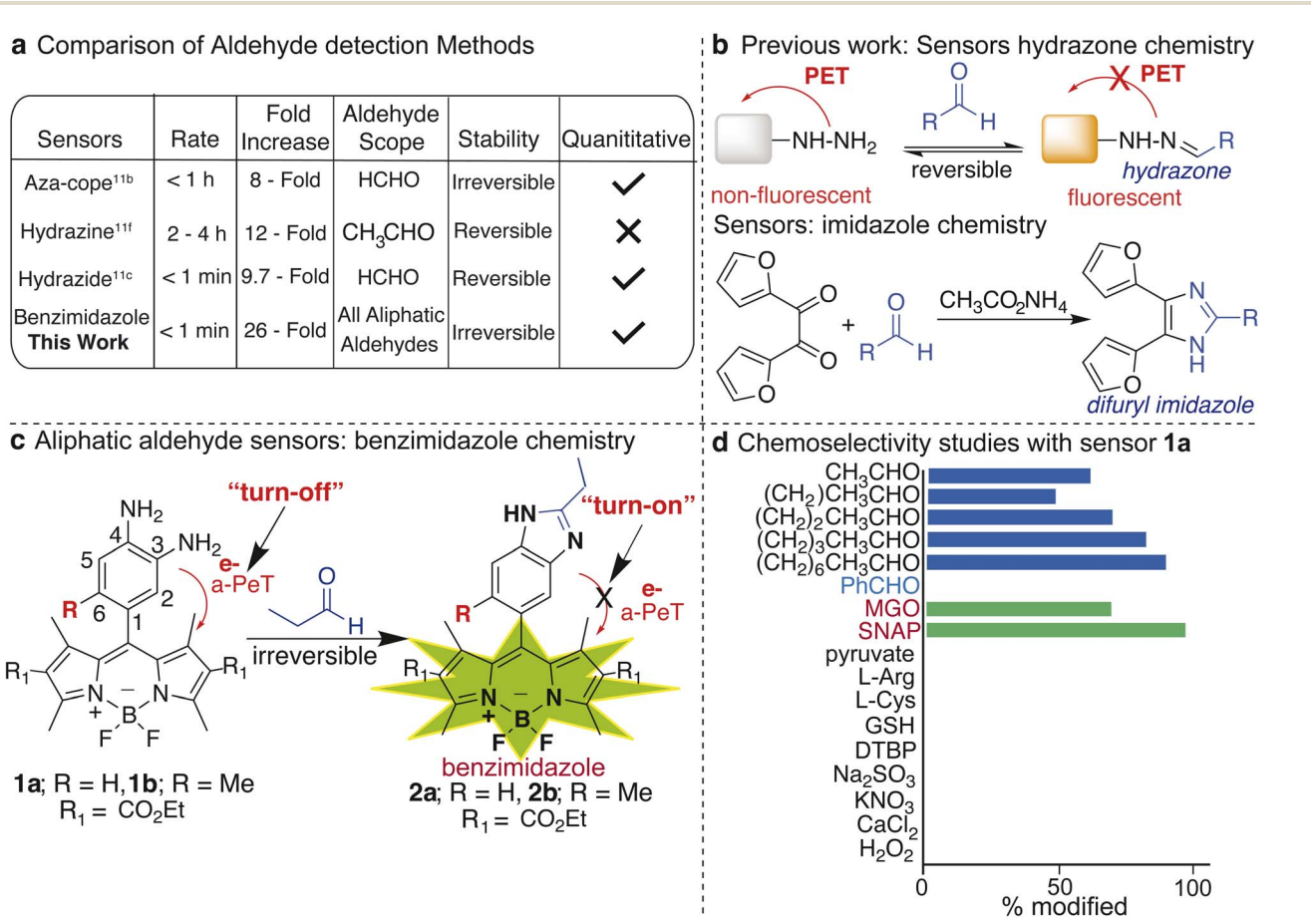

Fig. 1 Turn-on fluorescent sensors for detecting aliphatic aldehydes. (a) Comparison of previous aldehyde sensors with our work. Fold increase was calculated based on the quantum yield differences between the unreacted probe and its benzimidazole product upon reaction with propanal. (b) Previous methods of detecting aldehydes by reversible hydrazone reaction and imidazole chemistry are limited for live cell imaging. (c) The reaction of BODIPY-diamine sensors **1a** and **1b** with propanal to generate turn-on benzimidazole products **2a** and **2b**. (d) Chemoselectivity studies of sensor **1a** with varying biological metabolites in solution.

concentrations of aliphatic aldehydes in live cells in the presence of both ALDH activators and inhibitors, which is unachievable with other known irreversible sensors. We also added aldehyde sponges inside live cells to demonstrate the selectivity of our sensors for detecting aldehydes.

Results and discussion

Design and development of chemical sensors for aliphatic aldehydes

Existing methods for detecting small-to-long chain aliphatic aldehydes usually involve reactions with phenylhydrazine derivatives[15] to generate phenylhydrazone, which are detected by HPLC and fluorimetry (Fig. 1b). These hydrazone sensors for detecting aldehydes in live cells are limited due to the slow rate of reaction and reversibility under physiological conditions.[11f,11g,11j,11k,15] Another reaction used for aldehyde detection by HPLC involves the use of 2,2′-furil and ammonium acetate which leads to the formation of a stable difuryl imidazole (Fig. 1b).[16]

We sought a method that would leverage the formation of stable imidazole products from aliphatic aldehydes to develop turn-on sensors in live cells. We chose BODIPY as the fluorophore in our sensor because of its neutral charge, lipophilicity-enhanced cell permeability, and favorable partitioning into biological membranes. These attributes make BODIPY a robust reporter for detecting biological metabolites inside live cells.[17] We planned to use one such sensor containing 3,4-phenyldiamine attached to the BODIPY core, 3,4-phenyldiamine-BODIPY ethylester **1a** (Fig. 1c). In these sensors, fluorescence is quenched *via* an intramolecular photoinduced electron transfer (PeT) from the phenyldiamine moiety to the BODIPY acceptor fluorophore in a process known as acceptor-excited photoinduced electron transfer (a-PeT).[13] These processes are prevented upon reaction with aldehydes, resulting in turn-on fluorescence. Previous studies have shown that the substitution of a methyl group (R) at the 6th position on the phenyl ring raises the LUMO energy without forcing a simultaneous increase in E_{HOMO},[14] exhibiting high fluorescence efficiency (Fig. 1c). Therefore, we synthesized both 3,4-phenyldiamine-BODIPY ethylester **1a** and 6-methyl substituted 3,4-phenyldiamine-BODIPY ethylester **1b** for detecting the aliphatic aldehydes in live cells (for detailed synthesis and products characterization by ^{1}H NMR, ^{13}C NMR, and HRMS see ESI Fig. 1, 2, 5, 14 and 15†).[13,14]

Quantum yield

Next, we carried out the reaction of sensor **1a** with propanal under physiological conditions and generated the stable benzimidazole-BODIPY **2a** as characterized by ^{1}H NMR, ^{13}C NMR, and HRMS (ESI Fig. 5, 14, and 15†). The product **2a** resulted in turn-on fluorescence with an emission wavelength of 507 nm. This resulted from the formation of benzimidazole, which lowers the HOMO energy and increases the LUMO energy of the product, thereby avoiding both a-PeT and donor-excited photoinduced electron transfer (d-PeT) processes. We next calculated and compared the quantum yield of both sensors **1a** (0.005) and **1b** (0.04) with their corresponding products upon reaction with propanal **2a** (0.13) and **2b** (0.33) (ESI Fig. 3 and 4†).

This study showed a 26-fold increase in the fluorescence of **2a** compared to **1a** and an 8.5-fold increase in the fluorescence of **2b** compared to **1b**, making sensor **1a** the more sensitive aliphatic aldehyde detector. This is a significant enhancement over the previous acetaldehyde DarkZone sensor, resulting in only a 12-fold increase in fluorescence.[11f]

Chemoselectivity studies with other biological metabolites

We explored the reactivity and selectivity of sensor **1a** with varying biological metabolites, such as glutathione (GSH), pyruvate, L-Arg, L-Cys, DL-Hcy, $CaCl_2$, KNO_3, Na_2SO_3, $NaNO_3$, H_2O_2, di-*tert* butyl peroxide (DTBP), and nitric oxide (NO) (Fig. 1d). We also tested the reactivity with varying aliphatic and aromatic aldehydes (formaldehyde, acetaldehyde, propanal, butanal, pentanal, octanal, decanal, benzaldehyde, and 4-nitrobenzaldehyde) and the dicarbonyl methylglyoxal (MGO) in DMSO. Following incubation of various biological metabolites at very high concentrations (50 mM) with sensor **1a** (1 mM) for 2 h, only aliphatic aldehydes (C_1–C_{10}), NO, and MGO led to modified products (Fig. 1d). We did not observe the formation of any products with other biological metabolites, including aromatic aldehydes.

Notably, regardless of the chain lengths, all the aliphatic aldehydes reacted with sensor **1a** and generated the corresponding benzimidazole products with a significant fluorescence increase *versus* the baseline (ESI Fig. 5†). The various aldehydes triggered the same turn-on response with negligible differences in fluorescence intensity, which would allow for total aliphatic aldehyde detection. This discovery led us to reach our goal of detecting total aliphatic aldehyde concentrations in live cells. The formation of benzimidazole products by the reactions between diamine sensor **1a** and aldehydes (propanal (C3) or decanal (C10)) was confirmed by ^{1}H NMR, ^{13}C NMR, and HRMS (ESI Fig. 5, 14, and 15†). We did not add any oxidant to the reaction mixture and still observed the formation of the benzimidazole product. This is most likely due to aromatization leading to the formation of the thermodynamically favorable benzimidazole product over the unoxidized product.

Rate of aliphatic aldehyde detection by sensor 1a *in situ* and in live cells

We next evaluated the sensitivity and kinetic properties of sensor **1a** when reacted with aldehydes. The pseudo-first-order rate constant for detecting propanal by sensor **1a** was obtained by recording the change in the fluorescence over time upon incubating 10 μM sensor **1a** with 1 μM propanal and was calculated to be 0.0103 s^{-1} (Fig. 2a). This reaction rate is significantly rapid as compared to previous hydrazone (k = 0.0065 s^{-1})[11d] and DarkZone (time = 2–4 h)[11f] aldehyde sensors, granting sensor **1a** the potential to capture dynamics of aldehyde trafficking with unprecedented temporal resolution (Fig. 2a). Encouraged by this, we desired to determine the sensitivity of sensor **1a** in a complex cell lysate mixture. We

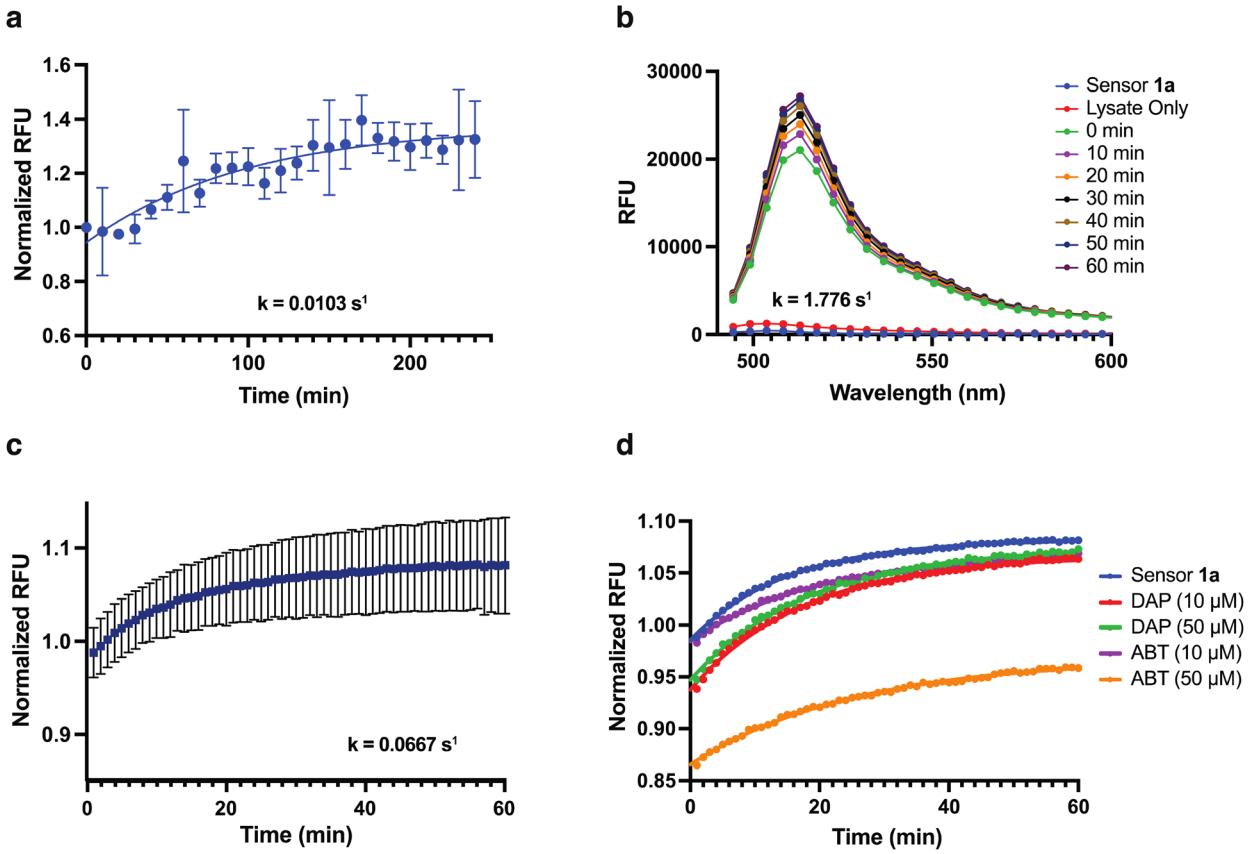

Fig. 2 Rate of detecting aliphatic aldehydes using sensor **1a**. (a) The reaction of sensor **1a** (10 μM) with propanal (1 μM) over 4 h. (b) Reaction of sensor **1a** with T47D cellular lysate for detecting endogenous aldehydes. (c) The reaction of sensor **1a** with endogenous aldehydes in live T47D cells measured in relative fluorescence units (RFU) normalized to sensor **1a**. The reaction was performed with 12 biological replicates. (d) Monitoring of changes in the total aliphatic aldehyde levels using sensor **1a** in T47D live cells in the presence of aldehyde sponges at different concentrations over time. RFU = relative fluorescence unit. Normalized RFU indicates RFU normalized to sensor **1a**. Time zero denotes the unreacted probe as a control. In (a) and (b), the reactions were done in triplicate. In (d), the reactions were done in four biological replicates. For clear visualization, the average of the trials is plotted in figures (b) and (d).

incubated 10 μM sensor **1a** with 50 μg of cell lysate extracted from the human breast ductal carcinoma cell line T47D and recorded the change in the fluorescence over time from endogenous aldehydes (Fig. 2b). To determine the sensitivity of sensor **1a** in detecting endogenous aliphatic aldehydes in live cells, we incubated sensor **1a** (5 μM) in live T47D cells and monitored the change in fluorescence over time (Fig. 2c). To detect the endogenous aldehyde dynamics in live cells, we incubated T47D cells with sensor **1a** (5 μM) and monitored changes in fluorescence over time in the presence of molecules that decrease cellular aldehyde levels (Fig. 2d). Notably, we observed the decrease in concentrations of endogenous aldehydes in the presence of aldehyde sponges (10–50 μM) (aldehyde reactive molecules) such as 2,3-diaminophenol (DAP) and 2-amino-4-chlorobenzenethiol (ABT) (Fig. 2d). ABT and DAP react with aldehydes and generate thiazolidine and benzimidazole, respectively, thus trapping aldehydes. As expected, in the presence of reactive aldehyde sponge at higher concentrations (ABT, 50 μM), a significant decrease in the fluorescence intensity was observed as compared to the less reactive aldehyde sponge at lower concentrations (DAP, 10 μM, Fig. 2d). Additionally, the reactivity of ABT is selective to aldehydes over nitric oxide. The decreased fluorescence signal in the presence of ABT confirmed that our probe is detecting aliphatic aldehydes over nitric oxide.

No additional cell death was observed as compared to the control for T47D cells treated with aldehyde sponges at varying concentrations (DAP and ABT, 10–50 μM, ESI Fig. 6†). These studies demonstrated the high sensitivity of sensor **1a** in monitoring changes in endogenous aldehyde levels in live cells.

Live-cell imaging of endogenous aliphatic aldehydes by sensor 1a

We examined the capacity of sensor **1a** to work inside live cells by first incubating T47D cells with varying concentrations of sensor **1a** (5–20 μM) for 24 h to determine the effect on cell death. We were pleased to observe no increase in cell death compared to the DMSO control in the range from 5 to 20 μM, as determined by flow cytometry (Fig. 3a, ESI Fig. 7†). This presents a significant improvement over previous aldehyde sensors that result in 20–30% cell death[11f] (Fig. 3a). Next, we incubated T47D cells with exogenous aldehydes, propanal, and acetaldehyde, at different concentrations (10 and 100 mM) and did not

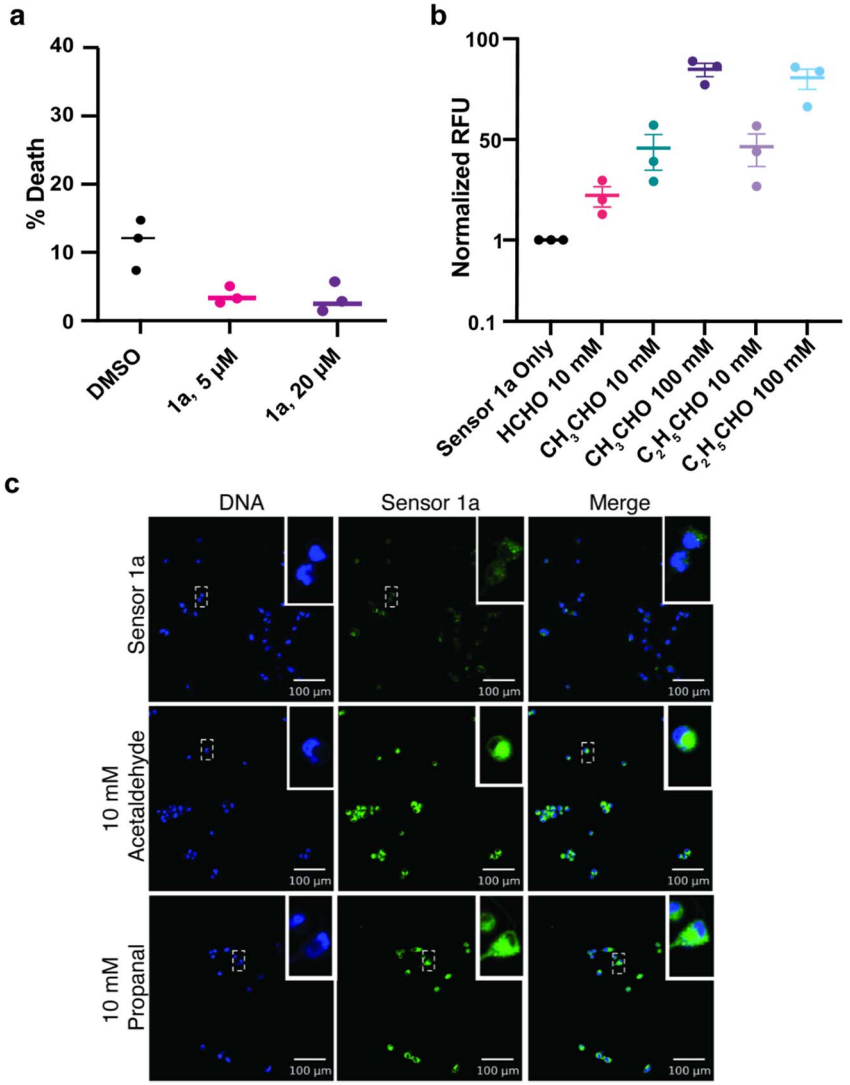

Fig. 3 Detection of exogenous aliphatic aldehydes by sensor **1a** in live cells. (a) Annexin V/PI staining of T47D cells incubated with sensor **1a** shows no increase in cell death as compared to the DMSO control. The DMSO control showed 5–10% variation in cell death. (b) Relative fluorescence units normalized to sensor **1a** after treatment of live cells with increasing concentration of exogenous aldehydes. (c) Live cell imaging of T47D cells after treatment with exogenous aldehydes, acetaldehyde (10 mM) and propanal (10 mM), in the presence of sensor **1a**. All experiments were performed in triplicate. Scale = 100 μM.

observe additional cell death in comparison to the DMSO control (ESI Fig. 8†).

To determine the ability of sensors to detect exogenously added aldehydes in live cells, we incubated cells with the sensor **1a** (5 μM) followed by treatment with acetaldehyde and propanal at the pathologically relevant range (10 mM and 100 mM) for an additional 1 h. An increase in the relative fluorescence for 10 mM aldehydes (45%) and for 100 mM aldehydes (95%) was readily detected in cells throughout the experiments using flow cytometry (Fig. 3b, ESI Fig. 9†). Next, we imaged the increase in the fluorescence in T47D cells with sensor **1a** (10 μM) in the presence of exogenous aldehydes, propanal and acetaldehyde (10 mM), using confocal microscopy (Fig. 3c). To determine the ability of the sensor to detect aldehydes in varying cell lines, we performed a similar experiment using live human prostate adenocarcinoma cells, LNCaP, and observed a similar increase in the fluorescence after the incubation of sensor **1a** (ESI Fig. 10†).

Limit of detection: quantification of changes in aldehyde levels inside live cells

Since we do not know the accurate concentrations of endogenous aldehydes inside cells, we used exogenous aldehydes to determine the accurate limit of detection for sensor **1a.** We quantified levels of propanal inside LNCaP cells with confocal microscopy. Sensor **1a** (10 μM) treated cells were incubated with increasing concentrations of propanal (0 μM, 2 μM, 4 μM, 6 μM, 8 μM, and 10 μM) for 1 h, followed by the measurement of fluorescence (Fig. 4a and ESI Fig. 11†). Relative fluorescence was calculated by analyzing pixel intensity to determine the fluorescence intensity

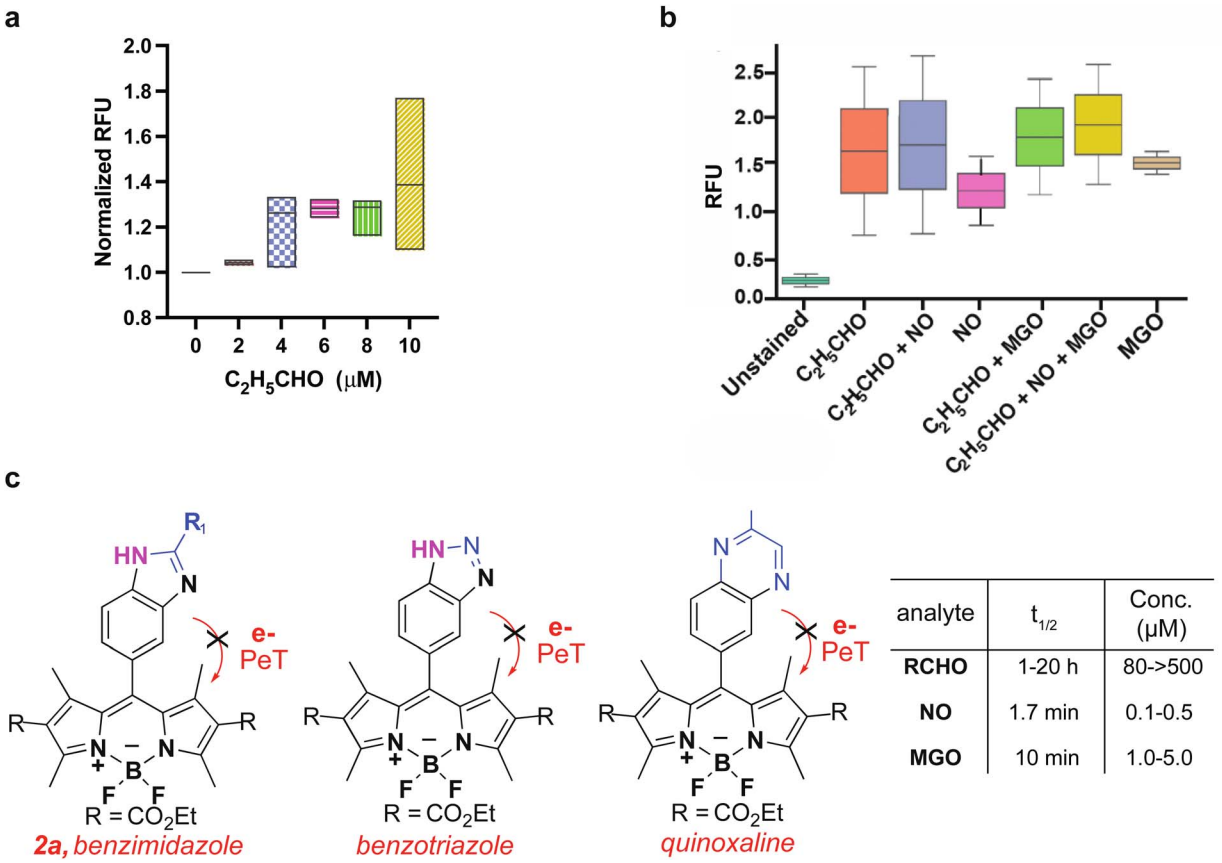

Fig. 4 Detection of aliphatic aldehydes by sensor **1a** in live cells. (a) Limit of detection experiments of sensor **1a** through incubation of varying concentrations of exogenous propanal (2–10 μM) inside live cells. (b) Selectivity and sensitivity of sensor **1a** to image propanal (20 μM) in live cells without interference from NO (0.5 μM) and MGO (5 μM). (c) Sensor **1a** product formation upon reactivity with aliphatic aldehydes, NO, or MGO. RFU = relative fluorescence unit. Normalized RFU indicates RFU normalized to sensor **1a**. All experiments were performed in triplicate.

of individual cells. We found that sensor **1a** exhibited a high dynamic range (2–10 μM) for detecting aliphatic aldehydes inside live cells. The previous DarkZone sensor showed no fluorescence inside cells even at 50 μM acetaldehyde concentration.[11f] Thus, sensor **1a** displays a significant increase in sensitivity and an impressive improvement in the limit of detection as compared to known aldehyde sensors.

Comparison of aldehyde detection with MGO and NO using sensor 1a

Since sensor **1a** is known to react with NO and MGO to create benzotriazole and quinoxaline fluorescence products, respectively[13,14] (Fig. 1d), we tested for the cross-reactivity of sensor **1a** with NO and MGO in live cells. We incubated LNCaP cells with sensor **1a**, followed by treatment with an NO donor (SNAP) or MGO at physiological concentrations for 1 h (Fig. 4b and ESI Fig. 12†). Cells exhibited only a minimal increase in fluorescence due to the formation of a benzotriazole product with NO (Fig. 4b). The lower physiological concentrations of NO (800 to 1000-fold lower) and much shorter half-life (~1.7 min)[13] as compared to total aliphatic aldehydes (~1–20 h)[18] precluded interference in the aliphatic aldehyde detection in live cells (Fig. 4b and c). Likewise, cells exhibited only a minimal increase in fluorescence due to the formation of a quinoxaline product with MGO (Fig. 4b and c). The estimated physiological concentration of MGO[17] is 80 to 100-fold lower than for total aliphatic aldehydes,[4] with a much shorter half-life (~10 min) (Fig. 4c).[1a] The shorter half-life of MGO is due to the high abundance and kinetic constant of the glyoxalase I enzyme (Glo1) responsible for the metabolism of MGO to non-toxic D-lactate in comparison to ALDH for aliphatic aldehydes.[1a] Taken together, these observations demonstrate that the physiological concentrations of MGO and NO do not interfere with the detection of aliphatic aldehydes by sensor **1a** in cellular settings (Fig. 4b). It is likely that the primary species (NO or MGO or total cellular aliphatic aldehydes) being detected is ultimately dependent on the system being studied and their relative concentrations, therefore appropriate controls (*e.g.* the addition of sponges or selective inhibitors for the relevant enzymes as shown in Fig. 2d, 5 and 6) are always needed to draw proper conclusions from the applications of these types of sensors.

Detection of acetaldehyde levels in preclinically relevant cancer models

Changes in cellular aldehyde levels occur in multiple diseases and often play a functional role in disease progression.

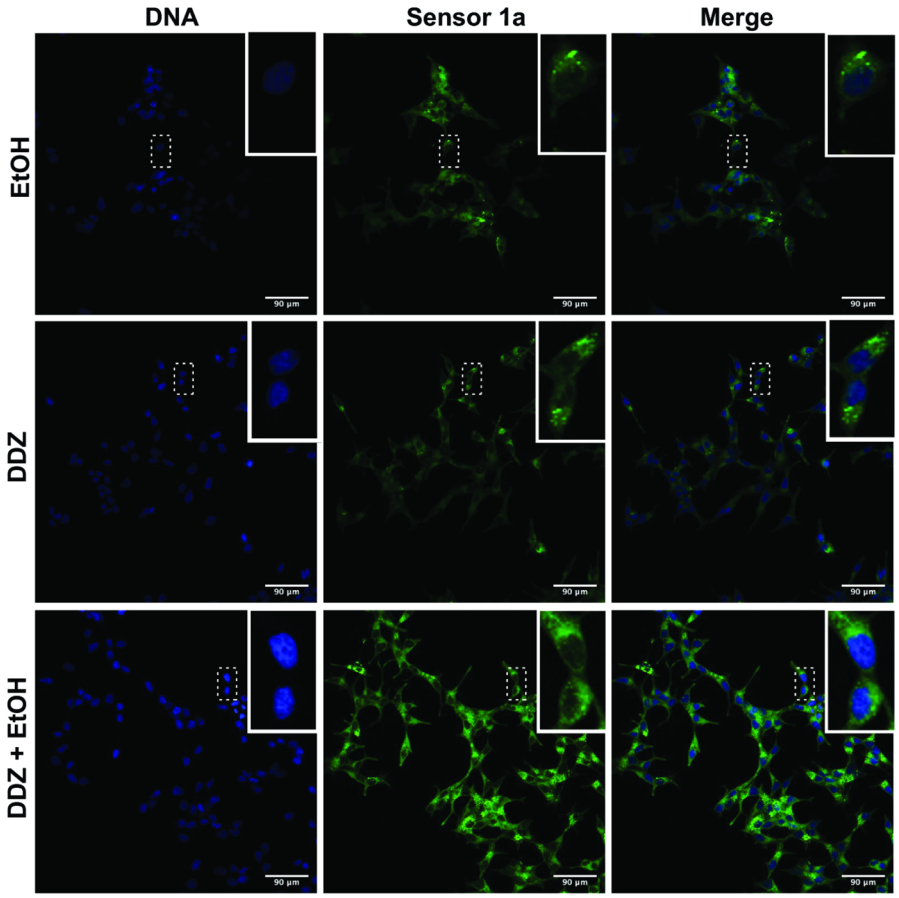

Fig. 5 Live cell imaging and monitoring of endogenous acetaldehyde production by sensor **1a**. The addition of EtOH in sensor **1a** pre-treated LNCaP cells increases fluorescence due to the endogenous production of acetaldehyde by a metabolic pathway inside the live cells. An increase in the fluorescence was observed in the presence of DDZ due to the inhibition of ALDH2-mediated metabolism of endogenous aldehydes to acids. A significant fluorescence increase was observed in the presence of both EtOH and DDZ due to production of more acetaldehyde by its metabolic pathway and the accumulation of aldehydes by inhibiting metabolism to acid. All these experiments are performed in triplicate. Scale = 90 μM.

ALDH2*2 mutation, affecting approximately >600 million people, is responsible for the accumulation of acetaldehyde after alcohol consumption, leading to disease states such as cancer, chronic liver damage, and Fanconi anemia (FA).[6,7] To test the ability of sensor **1a** to detect the endogenous production of aldehydes during the metabolic processes inside live cells, we incubated LNCaP cells with sensor **1a** (5 μM) followed by treatment with (i) ethanol, the metabolic precursor of acetaldehyde (10 mM), (ii) daidzin (DDZ), an ALDH2 inhibitor (5 μM), and (iii) both ethanol (10 mM) and DDZ (5 μM). Cells were imaged after 1 h to determine fluorescence intensity (Fig. 5). We found that LNCaP cells treated with ethanol showed a higher fluorescence signal as compared to the sensor **1a** treated control because of its metabolism to acetaldehyde. Notably, we also observed an increase in the cellular fluorescence following DDZ treatment because DDZ inhibits ALDH2, (mimicking ALDH2*2 mutation) thus increasing the accumulation of aldehydes from metabolic processes. In contrast, the previous DarkZone sensor for acetaldehyde did not show any change in fluorescence after the addition of excess DDZ (250 μM) or ethanol (2 mM).[11f] This is due to the slow reaction kinetics of the DarkZone sensor as compared to the metabolism of acetaldehyde. This study revealed that sensor **1a** has high sensitivity and fast kinetics suitable for detecting the endogenous production of acetaldehyde in live cells. In line with these results, we observed a significant increase in the fluorescence upon the addition of both ethanol and DDZ due to an increase in the production and the accumulation of acetaldehyde (Fig. 5). The fluorescent signals were cytosolic with no observed modification of the nucleus (Fig. 5).

Live-cell imaging and monitoring of medium-aliphatic aldehyde levels in the presence of both activator and inhibitor of ALDH2

In addition to acetaldehyde metabolism, ALDH2 plays an important role in mitigating oxidative stress by metabolizing other medium-to-long chain aliphatic aldehydes, including propanal.[19] Several studies have demonstrated that both ALDH2 upregulation and downregulation play a critical role in human cancers.[20] T47D cells cotreated with sensor **1a** (5 μM) and an activator (Alda-1) or an inhibitor (DDZ) of ALDH2 were used to

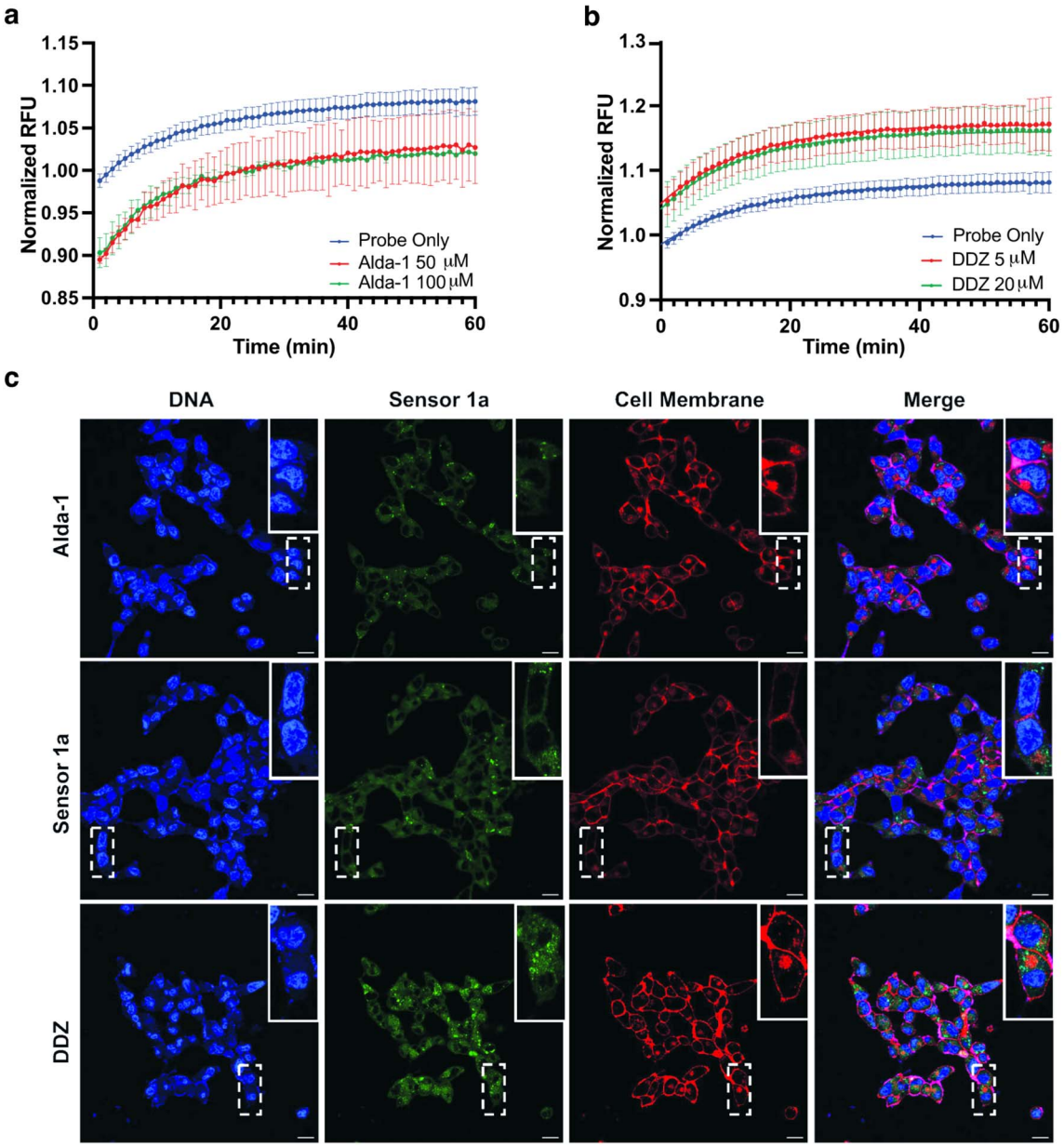

Fig. 6 Live cell imaging of endogenous aliphatic aldehyde levels by sensor **1a** in the presence of ALDH2 activator and inhibitor. (a) A decrease in fluorescence was observed in T47D cells incubated with **1a** due to the decrease in the concentrations of aldehydes in the presence of ALDH2 activator, Alda-1, over 1 h. (b) An increase in fluorescence was observed in T47D cells incubated with **1a** due to the increase in the concentrations of aldehydes in the presence of ALDH2 inhibitor, DDZ, over 1 h. (c) Confocal imaging of LNCaP cells cotreated with sensor **1a**, Alda-1, or DDZ. These experiments were done in triplicate. (a and b) Twelve trials were performed for these experiments, Alda-1 and DDZ were used at different concentrations due to their different affinities in activating or inhibiting ALDH2. Cell membrane visualization was performed with Cell Mask dye. The fluorescence was quantified and reported in the ESI.† RFU = relative fluorescence unit. Normalized RFU indicates RFU normalized to sensor **1a**. Time zero denotes unreacted probe as a control. Scale = 20 μM.

test the ability of sensor **1a** to detect such changes in concentrations of aldehydes in live cells, mimicking disease states. As expected, T47D cells treated with Alda-1 (50 μM and 100 μM) showed a decrease in the fluorescence signal as compared to sensor **1a** alone, owing to increased metabolism of endogenous aldehydes (Fig. 6a). We found that T47D cells treated with sensor **1a** in the presence of DDZ (5 μM and 20 μM) showed a higher fluorescence signal as compared to sensor **1a** due to the accumulation of aldehydes resulting from the inhibition of ALDH2 activity (Fig. 6b). Additionally, LNCaP cells treated with sensor **1a** and either Alda-1 or DDZ were imaged by confocal microscopy and showed a similar decrease (Fig. 6c, top) or increase (Fig. 6c, bottom) in fluorescence compared to sensor **1a** alone (Fig. 6c, middle) as quantified by analyzing the pixel intensity of the microscopy images (ESI Fig. 13†). We used LnCap cells for imaging because of their favorable morphology and better visualization of the aldehydes inside cells.

We also observed an immediate turn-on of the fluorescence inside live LnCaP cells upon addition of sensor **1a** as observed by live cell imaging over time (1–60 min, see the movie in the ESI†). This experimentation allowed the monitoring of sensor **1a** reactivity with available endogenous aldehydes inside the cell. The fast enzymatic activity of ALDH2 creates a small amount of endogenous aldehyde available for reactivity with sensor **1a**. These studies demonstrate the rapid cellular uptake of sensor **1a** and its fast reaction kinetics with aldehydes inside live cells.

These studies showed that sensor **1a** is non-toxic, exhibits high sensitivity and fast kinetics in detecting endogenous levels of aliphatic aldehydes in live cells, and is responsive to ALDH2 activity. This study further suggests the ability of sensor **1a** to monitor metabolic pathways that result in aldehyde production and diagnose disease states associated with changes in total aliphatic aldehyde levels.

Conclusions

In summary, we have shown that 3,4-phenyldiamine-BODIPY probe **1a** acts as a fluorescent sensor for selective and sensitive detection of small-to-long chain (C_1–C_{10}) total aliphatic aldehydes in live cells in the presence of other reactive biological metabolites. The condensation of probe **1a** with aliphatic aldehydes generates a benzimidazole moiety that lowers the HOMO energy and increases the LUMO energy, quenching both a-PeT and d-PeT processes and resulting in turn-on fluorescence at an emission wavelength of 507 nm. In contrast, the unreacted sensor showed almost no fluorescence because *o*-phenyldiamine acts as an electron donor in photo-electron transfer (PeT) quenching of BODIPY fluorescence. Sensor **1a** exhibits fast reaction kinetics ($k = 0.0667\ s^{-1}$) for detecting endogenous levels of aliphatic aldehydes in live cells with high sensitivity (26-fold increase in fluorescence) and high dynamic range (2 μM to 100 mM), thus enabling the detection of both physiological and pathological concentrations of aliphatic aldehydes in live cells without interference from competing biological analytes. The data presented herein showcase the broad applicability of sensor **1a** to image and measure changes in aliphatic aldehyde levels in a variety of common cell lines. Our sensors are non-cytotoxic, do not require any catalysts for completing the reaction, and generate an irreversible stable adduct with aliphatic aldehydes, which is in contrast to the known hydrazine-based DarkZone[11f] and naphthalimide sensors.[11e] We further demonstrated the ability of sensor **1a** to identify changes in the endogenous levels of aliphatic aldehydes in live mammalian cells by treating the cells with an activator (Alda-1) and inhibitor (DDZ) of ALDH2 enzyme, responsible for the metabolism of aldehydes, which is unachievable with other known sensors. We also showed a significant reduction in the fluorescence by the addition of aldehyde sponges that lead to the capture of free aldehydes. This study justifies the potential of sensor **1a** for quantifying, detecting, and monitoring changes in total aliphatic aldehyde concentrations over time in live cells, opening the opportunity to minutely dissect their roles and biological consequences in cellular metabolism and disease pathogenesis with impressive precision. Current efforts are underway to utilize this fluorescent sensor in monitoring various pathological states related to changes in total aliphatic aldehyde levels.

Data availability

The data supporting this article have been uploaded as part of the ESI.†

Author contributions

R. W. and M. R. designed the project. R. W. performed all the synthetic experiments and characterized the compounds by NMR and LCMS. P. C. and S. S. analyzed chemoselective reactions with sensor **1a**. J. F., J. S., and R. W. designed and performed all the live-cell experiments. J. S. helped in analyzing the live-cell data. All authors analyzed the results. R. W., P. C., and M. R. wrote the manuscript.

Conflicts of interest

There are no conflicts to declare.

Acknowledgements

This research was supported by a grant (Grant No. 1R35GM133719-01) from the National Institute of Health (NIH) and Alfred P. Sloan Foundation Award to M. R. Research reported in this publication was supported in part by the Emory University Integrated Cellular Imaging Core of the Winship Cancer Institute of Emory University and NIH/NCI under award number 2P30CA138292-04.

Notes and references

1 (*a*) R. P. Dator, M. J. Solivio, P. W. Villalta and S. Balbo, *Toxics*, 2019, **7**, 32; (*b*) P. J. O'Brien, A. G. Siraki and N. Shangari, *Crit. Rev. Toxicol.*, 2015, **35**, 609; (*c*) S. K. Brown, *Indoor Air*, 1999, **9**, 209; (*d*) J. Hahn, Y. B. Monakhova, J. Hengen, M. Kohl-Himmelseher, J. Schüssler, H. Hahn, T. Kuballa and D. W. Lachenmeier, *Tob. Induced Dis.*, 2014, **12**, 23; (*e*) V. M. Osorio and Z. L. Cardeal, *J. Braz. Chem. Soc.*, 2013, **24**, 1711.

2 (*a*) T. Finkel and N. J. Holbrook, *Nature*, 2000, **408**, 239; (*b*) M. T. Lin and M. F. Beal, *Nature*, 2006, **443**, 787.

3 (*a*) A. Yokoyama, E. Tsutsumi, H. Imazeki, Y. Suwa, C. Nakamura, T. Mizukami and T. Yokoyama, *Alcohol: Clin. Exp. Res.*, 2008, **32**, 1607; (*b*) Y. Li, A. Steppi, Y. Zhou, F. Mao, P. C. Miller, M. M. He, T. Zhao, Q. Sun and J. Zhang, *Sci. Rep.*, 2017, **7**, 4747.

4 S. A. Marchitti, C. Brocker, D. Stagos and V. Vasiliou, *Expert Opin. Drug Metab. Toxicol.*, 2008, **4**, 697.

5 (*a*) M. W. Weng, H. W. Lee, S. H. Park, Y. Hu, H. T. Wang, L. C. Chen, W. N. Rom, W. C. Huang, H. Lepor, X. R. Wu, C. S. Yang and M. S. Tang, *Proc. Natl. Acad. Sci. U. S. A.*, 2018, **115**, E6152; (*b*) J. I. Garaycoechea, G. P. Crossan,

F. Langevin, L. Mulderrig, S. Louzada, F. Yang, G. Guilbaud, N. Park, S. Roerink, S. Nik-Zainal, M. R. Stratton and K. J. Patel, *Nature*, 2018, **553**, 171; (*c*) S. C. Trewick, T. F. Henshaw, R. P. Hausinger, T. Lindahl and B. Sedgwick, *Nature*, 2002, **419**, 174.

6 A. Yoshida, I. Y. Huang and M. Ikawa, *Proc. Natl. Acad. Sci. U. S. A.*, 1984, **81**, 258.

7 (*a*) Y. C. Chao, S. R. Liou, S. F. Tsai and S. J. Yin, *Proc. Natl. Sci. Counc., Repub. China, Part B: Basic Sci.*, 1993, **17**, 98; (*b*) H. W. Goedde, D. P. Agarwal, G. Fritze, D. Meier-Tackmann, S. Singh, G. Beckmann, K. Bhatia, L. Z. Chen, B. Fang and R. Lisker, *Hum. Genet.*, 1992, **88**, 344; (*c*) S. E. Luczak, B. Elvine-Kreis, S. H. Shea, L. G. Carr and T. L. Wall, *J. Stud. Alcohol*, 2002, **63**, 74.

8 (*a*) C. Zwiener, T. Glauner and F. Frimmel, *Anal. Bioanal. Chem.*, 2002, **372**, 615; (*b*) Y. Chi, Y. Feng, S. Wen, H. Lu, Z. Yu, W. Zhang, G. Sheng and J. Fu, *Talanta*, 2007, **72**, 539; (*c*) S. M. Ochs, M. Fasciotti and A. D. P. Netto, *J. Spectrosc.*, 2015, **2015**, 1; (*d*) C. E. Baños and M. Silva, *J. Chromatogr. B: Anal. Technol. Biomed. Life Sci.*, 2010, **878**, 653.

9 (*a*) K. Yagi, *Biochem. Med.*, 1976, **15**, 212; (*b*) D. Del Rio, N. Pellegrini, B. Colombi, M. Bianchi, M. Serafini, F. Torta, M. Tegoni, M. Musci and F. Brighenti, *Clin. Chem.*, 2003, **49**, 690; (*c*) A. N. Ramdzan, M. I. G. S. Almeida, M. J. McCullough and S. D. Kolev, *Anal. Chim. Acta*, 2016, **919**, 47; (*d*) J. Zhang, H. Zhang, M. Li, D. Zhang, Q. Chu and J. Ye, *J. Chromatogr. A*, 2010, **1217**, 5124.

10 (*a*) S. Wang, H. M. Ang and M. O. Tade, *Environ. Int.*, 2007, **33**, 694; (*b*) Y. Cho, M. K. Song, T. S. Kim and J. C. Ryu, *Sci. Rep.*, 2018, **8**, 10497.

11 (*a*) T. F. Brewer, G. Burgos-Barragan, N. Wit, K. J. Patel and C. J. Chang, *Chem. Sci.*, 2017, **8**, 4073; (*b*) T. F. Brewer and C. J. Chang, *J. Am. Chem. Soc.*, 2015, **137**, 10886; (*c*) X. G. Liang, B. Chen, L. X. Shao, J. Cheng, M. Z. Huang, Y. Chen, Y. Z. Hu, Y. F. Han, F. Han and X. Li, *Theranostics*, 2017, **7**, 2305; (*d*) Y. Tang, X. Kong, A. Xu, B. Dong and W. Lin, *Angew. Chem., Int. Ed.*, 2016, **55**, 3356; *Angew. Chem.*, 2016, **128**, 3417; (*e*) P. Jin, C. Jiao, Z. Guo, Y. He, S. Zhu, H. Tian and W. Zhu, *Chem. Sci.*, 2014, **5**, 4012; (*f*) L. H. Yuen, N. S. Saxena, H. S. Park, K. Weinberg and E. T. Kool, *ACS Chem. Biol.*, 2016, **11**, 2312; (*g*) D. Larsen, A. M. Kietrys, S. A. Clark, H. S. Park, A. Ekebergh and E. T. Kool, *Chem. Sci.*, 2018, **9**, 5252; (*h*) L. He, X. Yang, M. Ren, X. Kong, Y. Liu and W. Lin, *Chem. Commun.*, 2016, **52**, 9582; (*i*) C. Liu, X. Jiao, S. He, L. Zhao and X. Zeng, *Dyes Pigm.*, 2017, **138**, 23; (*j*) M. Suchý, C. Lazurko, A. Kirby, T. Dang, G. Liu and A. J. Shuhendler, *Org. Biomol. Chem.*, 2019, **17**, 1843; (*k*) C. Lazurko, I. Radonjic, M. Suchý, G. Liu, A. Rolland-Lagan and A. J. Shuhendler, *ChemBioChem*, 2019, **20**, 543.

12 R. M. LoPachin and T. Gavin, *Chem. Res. Toxicol.*, 2014, **27**, 1081.

13 (*a*) Y. Gabe, Y. Urano, K. Kikuchi, H. Kojima and T. Nagano, *J. Am. Chem. Soc.*, 2004, **126**, 3357; (*b*) H. X. Zhang, J. B. Chen, X. F. Guo, H. Wang and H. S. Zhang, *Anal. Chem.*, 2014, **86**, 3115.

14 T. Wang, E. F. Douglass, K. J. Fitzgerald and D. A. Spiegel, *J. Am. Chem. Soc.*, 2013, **135**, 12429.

15 X. J. Xiong, H. Wang, W. B. Rao, X. F. Guo and H. S. Zhang, *J. Chromatogr. A*, 2010, **1217**, 49.

16 M. F. B. Ali, N. Kishikawa, K. Ohyama, H. A. M. Mohamed, H. M. Abdel-Wadood, A. M. Mohamed and N. Kuroda, *J. Chromatogr. A*, 2013, **1300**, 199.

17 (*a*) G. Ulrich, R. Ziessel and A. Harriman, *Angew. Chem., Int. Ed.*, 2008, **47**, 1184; (*b*) N. Boens, B. Verbelen and W. Dehaen, *Eur. J. Org. Chem.*, 2015, **2015**, 6577; (*c*) T. Kowada, H. Maeda and K. Kikuchi, *Chem. Soc. Rev.*, 2015, **44**, 4953.

18 (*a*) L. K. Silva, G. A. Hile, K. M. Capella, M. F. Espenship, M. M. Smith, V. R. De Jesuś and B. C. Blount, *Environ. Sci. Technol.*, 2018, **52**, 10571; (*b*) J. L. Dorne, C. Bechaux, G. Kass and M. Innocenti, *EFSA J.*, 2014, **12**, 3550.

19 C. E. Graham, K. Brocklehurst, R. W. Pickersgill and M. J. Warren, *Biochem. J.*, 2006, **394**, 67.

20 (*a*) B. N. Rexer, W. L. Zheng and D. E. Ong, *Cancer Res.*, 2001, **61**, 7065; (*b*) J. G. Koch, X. Gu, Y. Han, A. K. El-Naggar, M. V. Olson, D. Medina, D. J. Jerry, A. C. Blackburn, G. Peltz, C. I. Amos and G. Lozano, *Mamm. Genome*, 2007, **18**, 300.